Fuel 254 (2019) 115678

Contents lists available at ScienceDirect

Fuel

journal homepage: www.elsevier.com/locate/fuel

Full Length Article

Impact of the surrogate formulation on 3D CFD engine knock prediction using detailed chemistry

Corinna Netzer[a,*], Lars Seidel[b,*], Frédéric Ravet[c], Fabian Mauß[a]

[a] Brandenburg University of Technology, Germany
[b] LOGE Deutschland GmbH, Germany
[c] Renault SAS, France

ARTICLE INFO

Keywords:
Detailed chemistry
Surrogate
ETRF
Engine knock
CFD
Resonance theory

ABSTRACT

For engine knock prediction, surrogate fuels are often composed of *iso*-octane and *n*-heptane since they are the components of the Primary Reference Fuel (PRF). By definition, a PRF has no octane sensitivity (S = RON-MON). However, for a commercial gasoline fuel holds RON > MON and therefor S > 0. More complex surrogates are Toluene Reference Fuels (TRF) and Ethanol containing Toluene Reference Fuels (ETRF). In this work, the impact of the surrogate formulation on the prediction of flame propagation and auto-ignition in the unburnt gases are investigated. The surrogates are composed such that the Research Octane Number is the same. The auto-ignition events ahead of the flame front are predicted using 3D CFD and a combustion model based on the ETRF mechanism by Seidel (2017). The strength of the auto-ignition is determined using the detonation diagram by Bradley and co-workers (2002, 2003). Applying the different surrogates, ignition kernels of different size and reactivity are predicted. The results indicate a dependency on the local temperature history and the low temperature chemistry of the fuel species. The comparison of homogenous constant volume reactor and transient simulations show that the analysis of ignition delay time and octane rating solely from homogenous simulations is not sufficient if the knock tendency of a surrogate in engine simulations needs to be characterized.

1. Introduction

The fuel properties of a commercial gasoline fuel have a major impact on engine knock [1–3]. The fuels' resistance to auto-ignition is characterized by the octane rating. The octane rating relates the tested commercial fuel against a mixture of *iso*-octane and *n*-heptane, called Primary Reference Fuel (PRF). Depending on the test conditions, defined in ASTM D2699/D2700 and EN ISO 5163/5164, the Research Octane Number (RON) or Motored Octane Number (MON) are found [1,3]. RON and MON are defined as the *iso*-octane volume fraction of the PRF blend that leads to the same knock-meter reading as the tested fuel. By definition:

$$RON_{iso-octane} = MON_{iso-octane} = 100 \quad (1)$$

$$RON_{n-heptane} = MON_{n-heptane} = 0. \quad (2)$$

As consequence of this definition, the RON and MON of a PRF are the same, but commercial gasolines have in general higher RON than MON. This difference is called octane sensitivity S:

$$S = RON - MON \quad (3)$$

To respect this discrepancy, the combination of RON and MON to the anti-knock index AKI is frequently used [4]:

$$AKI = \frac{1}{2}(RON + MON) \quad (4)$$

In modern direct injection spark ignition engines (DISI, manufactured after 1990) employing strategies such as downsizing, turbocharging, valve overlapping and charge cooling, the temperatures of the unburnt zone are today 100 K below the RON test conditions and 250 K below the MON conditions for a given end gas pressure under knocking conditions [5]. However, those numbers depend on the boosting level, scavenging and charge cooling [5]. Therefore, the knock tendency prediction moves away from MON conditions. RON test like conditions are more dominating whereas the auto-ignition tendency is lower than in the cooperative fuel research engine [5,6]. To reflect the impact of the operating conditions on the knock probability, the octane index (OI) using the *K*-factor was developed [6,7]:

$$OI = RON - K(RON - MON) \quad (5)$$

K depends on the engine and operating conditions and needs

* Corresponding authors.
E-mail addresses: corinna.netzer@b-tu.de (C. Netzer), lars.seidel@logesoft.com (L. Seidel).

https://doi.org/10.1016/j.fuel.2019.115678
Received 26 November 2018; Received in revised form 18 January 2019; Accepted 18 June 2019
Available online 27 June 2019

therefore to be determined empirically for each engine [6]. In experiments, the knock limit spark advance (KLSA) for different fuels with different octane sensitivity is determined and K correlated. For modern engines, K is mostly negative, which leads to $OI > RON$, or to small positive values $K < 0.2$ [7]. Higher speeds lead to an increase of K, hence the MON contribution to OI increases with speed [6,8].

In simulations, the surrogate fuel must be formulated in a way that it represents the auto-ignition tendency of the commercial gasoline fuel, since the fuel octane rating has a major impact on auto-ignition. To consider fuel blend effects, modeling approaches with varying details are available in literature. The use of a global chemical mechanism and an adequate fitting procedure for auto-ignition prediction are proposed, for instance in the Shell model [9–11]. With the use of (reduced) reaction mechanisms, the oxidation of the fuel species is described in more detail. Frequently, Primary Reference Fuels (PRF) are applied to predict engine knock. Their composition of *iso*-octane (RON = 100, MON = 100) and *n*-heptane (RON = 0, MON = 0) can be used to compose a surrogate that represents the RON of a commercial gasoline fuel, but never at the same time the correct MON or octane sensitivity S. With this rather simple surrogate fuel model, auto-ignition can be reproduced, for instance demonstrated in Teodosio et al. [12], but the PRF model does not capture the major chemical and physical properties of commercial gasoline such as ethanol and aromatic content or C:H:O-ratio. To reproduce these properties, the use of ethanol toluene reference fuels (ETRF) was suggested [13-15]. This surrogate fuel is a blend of *n*-heptane, *iso*-octane, toluene and ethanol. A reaction mechanism describing the combustion of an ETRF surrogate caters for the prediction of the impact of chemical and physical gasoline properties on auto-ignition. In contrast to fitted correlation, detailed chemistry can also capture the impact of exhaust gas recirculation (EGR), in particular radicals or NOx in the residual gas discussed, for example, in the works by Stenlåås et al. [16] and Hoffmeyer et al. [17] and references therein. Therefore, ETRF reaction schemes are today the best compromise to define a flexible surrogate fuel for gasoline with high accuracy while keeping the number of surrogate components low [17].

Further, such detailed reaction schemes can be applied to predict the laminar flame speed, which is an important input parameter for the flame propagation prediction. Often, this parameter is taken from correlations, as for example by Gülder et al. [18] or Metghalchi and Keck [19]. Those correlations can replicate the change of the reference laminar flame speed s_l^0 on pressure p, unburnt temperate Tu, fuel/air equivalence ratio ϕ or dilution. Very specific fuel effects, such as the location of the maximum laminar flame speed that depends on the ongoing reactions and oxygen demand or the impact of aromatic or alcohol content, cannot be covered by generalized correlations.

In this work, surrogates composed of different number of species (PRF, TRF, ETRF) are compared to each other. The composed surrogates have all the same RON, but differ in MON and other characteristics such as C:H:O–ratio, lower heating value (LHV) and density. Through this analysis, the impact of the surrogate formulation on flame propagation and auto-ignition occurrence and strength is analyzed.

In the first part the models for flame propagation and auto-ignition prediction and the classification methodology for the auto-ignitions are presented, followed by the discussion on the analyzed surrogates. The analysis part, first deals with the impact on flame propagation prediction, secondly discusses the auto-ignition prediction using same fuel and air masses and third the auto-ignition prediction using same fuel/air-equivalence ratios ϕ.

2. Methodology

Flame propagation is predicted using the G-equation model [20]. It was chosen since this is a detailed model for the turbulent flame propagation based on properties of macro and microscales. Further, the turbulent flame speed model is based on provided laminar flame speeds. By the use of laminar flame speed tables, compiled using a detailed reaction scheme, the model allows for a direct connection between detailed chemistry and flame propagation prediction.

Besides the capability to predict flame propagation, the combustion model needs to predict auto-ignition in the unburnt zone, which is a prerequisite for engine knock prediction. The G-equation model includes no formulation for the prediction of auto-ignition. Anyway, flame propagation and auto-ignition in the unburnt zone, are from the chemical point of view independent processes that do not need to be modeled with the same combustion model. Since the unburnt zone is rather homogeneous in SI engines, a homogeneous approach – the Well-Stirred-Reactor (WSR) model [21] – is applied. Each cell in the unburnt zone is treated as a WSR, hence with sufficient discretization local inhomogeneity are accounted for. For SI engines, this approach is well established and widely used, see for example [22–25] and references therein.

The combustion processes are predicted using the ETRF reaction scheme by Seidel [26], which was developed using the core model from Seidel et al. [27] and following the rates by Ahmed et al. [28]. The detailed reaction scheme did consist of 352 species. To reduce the number of species the chemistry-guided reduction concept by Zeuch et al. [29], which was further developed with special emphasis on engine simulation by Seidel et al. [30] was applied. Since auto-ignition and the flame propagation are physically independent and modeled as separate processes, it was decided to split up the reduction process to these two targets [20,31,32]. The reduced scheme for prediction of auto-ignition consists of 188 species and is used within the WSR model. The reaction scheme for laminar flame speed is reduced to 78 species and used to compile the flame speed look-up tables.

A post-processing strategy is applied to evaluate the character and the severity of the auto-ignition event based on the detonation diagram by Bradley and co-workers [33–36]. Typically used knock indexes are calculated from the pressure fluctuations [37]. In contrast, the use of the detonation theory enables to analyse the auto-ignition in the unburned mixture, which is the origin of those pressure gradients. By the use of the regime classification, a distinction between auto-ignition events in deflagration and transition to harmful developing detonation, which corresponds in engines to knocking combustion, is possible. In the detonation diagram, the resonance parameter ξ and the reactivity parameter ε characterize the auto-ignition mode:

$$\xi = \frac{a}{u_a} \tag{6}$$

$$u_a = \frac{\partial r}{\partial \tau} \tag{7}$$

$$\varepsilon = \frac{r_0}{a\tau_e} \tag{8}$$

The resonance parameter is given by the ratio of the imposed gas velocity u_a to the speed of sound a. If the two speeds are in the same order of magnitude, the two waves may combine and form a developing detonation. The reactivity parameter includes the initial radius of the ignition kernel r_0 and is a measure for the hot spot reactivity. The resonance and the reactivity parameter have a direct dependency on fuel characteristics in terms of the ignition delay time τ and the excitation time τ_e. The borders of the developing detonation peninsula and engine relevant regimes are given in Fig. 1. Peters et al. [38] verified the developing detonation boundaries for *n*-heptane and *iso*-octane-air mixtures to be close to the original ones derived for a H_2/CO/air mixture and confirmed the minimum for the reactivity parameter $\varepsilon = 1.6$. A fuel with negative temperature coefficient and a pronounced low temperature chemistry is more likely to develop an auto-ignition, but a developed and visible ignition kernel with significant heat release already passed through the low temperature regime. The ignition of this kernel that may lead to a developing detonation is driven by the high temperature regime. Therefore, the high temperature chemistry is the reason for the apparent fuel independence of the transition boundaries,

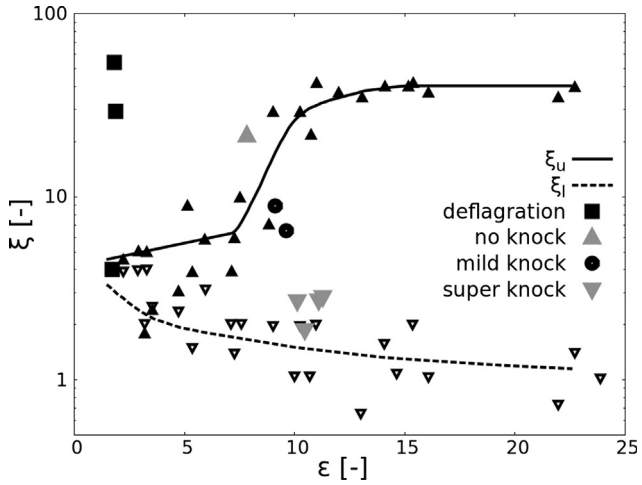

Fig. 1. Detonation diagram peninsula and corresponding engine conditions. Upper and lower peninsula by Bradley et al. [33]. Colored symbols by Kalghatgi et al. [35] and Bates et al. [39].

since the high temperature chemistry is similar for the analyzed fuels as found in [38].

In the 3D CFD post-processing the ignition kernel size is measured and the thermodynamic properties such as hot spot temperature elevation are extracted. Ignition delay times τ and excitation times τ_e are calculated using constant volume reactors [40]. The post-processing strategy is introduced and in detail discussed in [31].

The analysis is carried out using a turbocharged spark ignition Renault passenger car engine with port-injection. The spark is initialized 4 °CA before top dead center (TDC), which was found in the experiments to be the KLSA using a commercial gasoline with RON 94.5/MON 84.1 (more details in Tables 2 and A2, commercial gasoline no. 14). The engine geometry is given in Table 1. The focus of this work is to study the impact of the chemistry and the surrogate formulation on engine knock. The port-injection is not modelled to exclude the impact of vaporization. The simulations are initialized homogenous at inlet valve closure (IVC). The flow field and turbulence level are taken from an open cycle simulation and imposed at IVC. Reynolds-Averaged Navier-Stokes simulations (RANS) with a base mesh size of 0.75 mm are applied. Using the automatic mesh refinement (AMR) strategy [21] based on temperature and flow velocity, the mesh is refined at the flame front and chemical reactive regions down to 0.125 mm.

3. Surrogates

Different surrogates with same RON, but different number of surrogate fuel species and therefore different MON are composed using the methodology developed in [26] based on the Modified Linear by Volume (MLbV) correlation by Morgan et al. [13] and mixing rules for oxygenated molecules by Anderson et al. [41]. In the experiment, a commercial gasoline without ethanol content was used (commercial gasoline no. 14 in Table A4). Accounting the aromatic content of this gasoline to toluene, setting the ethanol content in the surrogate to zero and calculating the *iso*-octane and *n*-heptane content according to [13,26,41] results in a TRF surrogate that agrees well in density, LHV and C:H:O-ratio with the commercial gasoline. However, the octane sensitivity is under-predicted (Table 2). To investigate different surrogate formulations, a PRF is composed neglecting the aromatic content of the commercial gasoline. As discussed before, the PRF surrogate has no octane sensitivity. The LHV (per mass) for this surrogate is the highest compared to the other surrogates. Since European gasoline fuels usually contain ethanol, ETRF surrogates adopting the properties of the commercial gasoline with 5% and 10% ethanol by volume are composed, here named “ETRF 1” and “ETRF 2”. To match the target RON, the *iso*-octane and toluene content need to be aligned. To generate a surrogate with the same sensitivity as the commercial gasoline the surrogate “ETRF 3” with an increased toluene content is formulated. However, this results in the lowest LHV per mass among the surrogates. The surrogate compositions are summarized in Table 3.

Table 1
Engine geometry and operating conditions.

Bore	72.0 mm
Stroke	82.0 mm
Connecting rod length	128.0 mm
Compression ratio	10.9
Speed	2000 rpm
Spark timing	−4 °CA aTDC
IMEP	10.6 bar
IVO/IVC	−410.0/−100.0 °CA aTDC
EVO/EVC	120.0/390 °CA aTDC

4. Results and discussion

4.1. Impact of the surrogate formulation on the flame propagation prediction

In a first step, the impact of the surrogate properties on the flame propagation are investigated. For this purpose, a flame speed look-up table for each surrogate was compiled. The laminar flame speeds of the surrogate components and the surrogates are shown at 60 bar in Figs. 2 and 3. At stoichiometric conditions the PRF surrogate has the highest laminar flame speed. The TRF and ETRF surrogates have slower flame speeds due to their toluene content.

To analyze the impact on flame propagation, chemistry dependencies of the surrogate in unburnt and burnt zone are excluded. This is achieved by initializing all cases with the same surrogate, but applying different flame speed tables. Surrogate “TRF” is chosen to be initialized since it is composed according to the fuel used in the experiment. The same clear difference between the PRF surrogate and the other surrogates are found in the engine simulation (Fig. 4). It has to be noted that the CFD simulation has been calibrated using the TRF surrogate, therefore no conclusions on which surrogate leads to the most accurate combustion prediction should be drawn, instead the trends should be considered. Table 4 provides a quantification of the difference in flame propagation. For that purpose, the peak pressure and its location and the combustion phasing at 5%, 10%, 50% and 90% burn duration normalized to the experiment are calculated. The simulation using surrogate “TRF” shows the best agreement with the experiment thanks to the discussed setup choice. Surrogate “PRF” over-predicts the combustion rate, whereas the other surrogates under-predict. At the center of combustion (CA_{50}, in Table 4) the maximum difference between the fastest (PRF) and the slowest (ETRF 1) surrogates are 1.5 °CA. The maximal difference in peak pressure is about 3.5 bar. From this analysis, it can be concluded that it is important to consider the impact of fuel composition on the flame speed prediction in engine simulations.

4.2. Impact on engine knock prediction assuming constant fuel mass

In a second step, the impact of the surrogate formulation on engine knock is examined. This work does not aim to optimize a fuel or surrogate, but to understand how the surrogate composition may affect the knock prediction. Two different studies that keep all operating parameter the same, are carried out: first the fuel surrogate mass is kept constant and secondly the equivalence ratio is kept constant. Load change and port-injection are not modelled to reduce the number of influencing factors. All simulations are started with same initial mean temperature and pressure. The operating conditions are kept the same. These assumptions lead to a carburetor-type setup, analyzing the same surrogate applying a direct injection might change the results.

Table 2
Properties of the commercial gasoline (fuel analysis) and the surrogates (calculated) all with RON = 94.5.

	MON [–]	S [–]	Aromatic content [vol.%]	Ethanol content [vol.%]	ρ [kg/m^3]	LHV [MJ/kg]	C:H:O-ratio [mass%]
Gasoline	84.1	10.4	32.6	0.0	747.5	42.9	86.9.13.1:0.0
PRF	94.5	0.0	0.0	0.0	691.3	44.4	84.2:15.8:0.0
TRF	88.2	6.3	32.6	0.0	747.3	42.9	86.9:13.1:0.0
ETRF 1	88.1	6.4	22.5	5.1	735.3	42.4	84.3:13.8:1.9
ETRF 2	87.6	7.0	15.8	10.1	728.5	41.7	82.0:14.2:3.8
ETRF 3	84.3	10.1	39.5	10.2	769.6	40.9	84.0:12.4:3.6

Table 3
Surrogate composition in mass percent.

	iso-octane	n-heptane	toluene	ethanol
PRF	94.6	5.4	0.0	0.0
TRF	49.5	12.7	37.8	0.0
ETRF 1	55.7	12.2	26.6	5.4
ETRF 2	57.9	12.3	18.8	11.0
ETRF 3	28.8	16.2	44.6	10.4

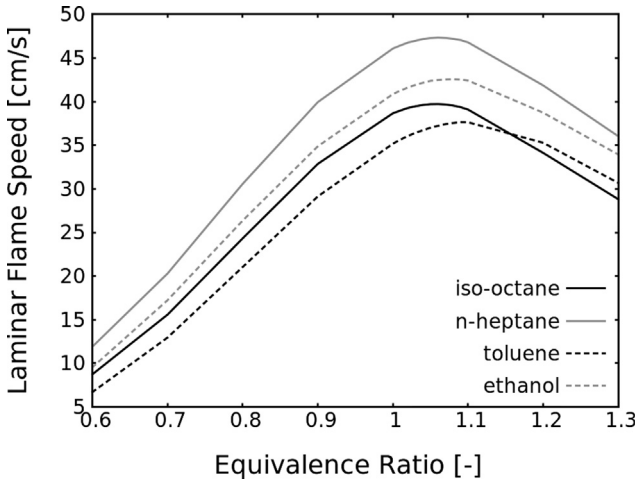

Fig. 2. Predicted laminar flame speed for the surrogate components at 60 bar and 600 K using the skeletal scheme for laminar flame speed prediction by Seidel [26].

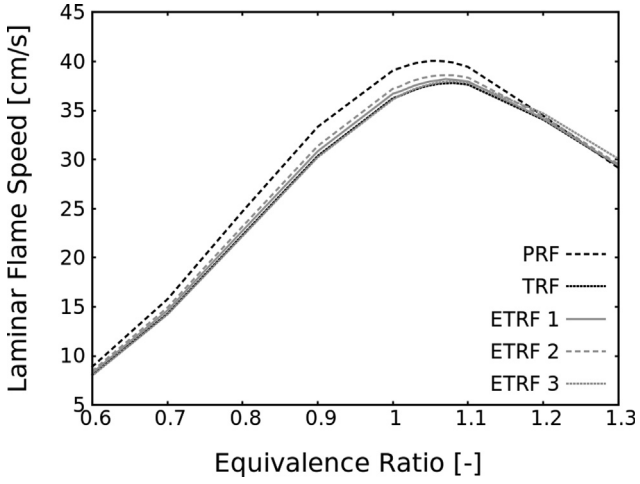

Fig. 3. Predicted laminar flame speed for the surrogates at 60 bar and 600 K using the skeletal scheme for laminar flame speed prediction by Seidel [26].

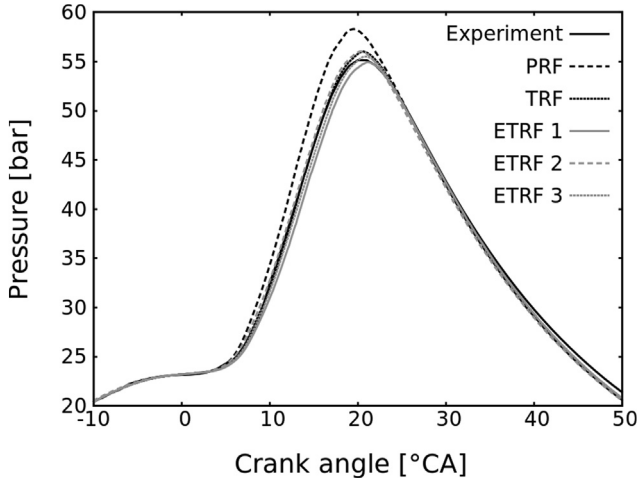

Fig. 4. Mean predicted pressure using the surrogate specific flame speed tables.

Table 4
Predicted location of the peak pressure and the combustion phasing related to the experiment. Analysis of the combustion prediction shown in Fig. 4.

		Experiment	PRF	TRF	ETRF1	ETRF2	ETRF3
CA_5	[°CA aTDC]	6.5	−0.1	0.2	0.5	0.3	0.4
CA_{10}	[°CA aTDC]	8.7	−0.7	−0.2	0.1	−0.2	−0.1
CA_{50}	[°CA aTDC]	15.3	−0.7	0.3	0.8	0.3	0.5
CA_{90}	[°CA aTDC]	24.5	−0.7	0.6	1.2	0.5	0.9
θ_{Pmax}	[°CA aTDC]	20.0	−0.5	0.5	1.2	0.5	0.9
P_{max}	[MPa]	55.2	3.1	0.8	−0.3	0.8	0.3

According to [7], this simulation setup causes the MON value to be more significant than in direct injection gasoline engines.

In the first study, the air and fuel mass in the cylinder for all surrogates are set to the same amount. The simulation is initialized homogenous at IVC, masses are not changed, all differences can be attributed to the chemistry. Since all surrogates have different C:H:O-ratio and consequently a different stoichiometric air demand, the fuel/air equivalence ratio ϕ differs about $\phi = 1 \pm 0.05$. There are also small deviations in trapped energy due to differences in LHV of the surrogates.

The second study explores the alternative to adjust the fuel surrogate mass so that all mixtures are stoichiometric. This leads to different trapped masses.

Ignition delay time prediction using constant volume reactors versus temperature are shown for the surrogate components in Fig. 5 and for the surrogate components in Figs. 6 and 7. The ignition delay time of surrogate “PRF” has a different trend than the TRF and ETRF surrogates. Whereas for $\phi = 1$ (dashed lines), the ignition delay time of the TRF and ETRF surrogates converge at 870 K and invert the trends at this temperature, this cross-over temperature for the actual trapped mixtures with different fuel/air equivalence ratios (solid lines) appears at about 820 K. The predicted ignition delay times are converted from

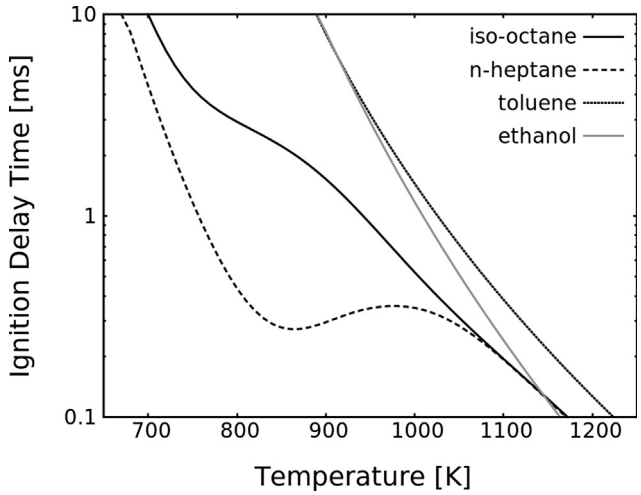

Fig. 5. Ignition delay time prediction of the surrogate species for $\phi = 1$ and 60 bar using the skeletal scheme for auto-ignition prediction by Seidel [26].

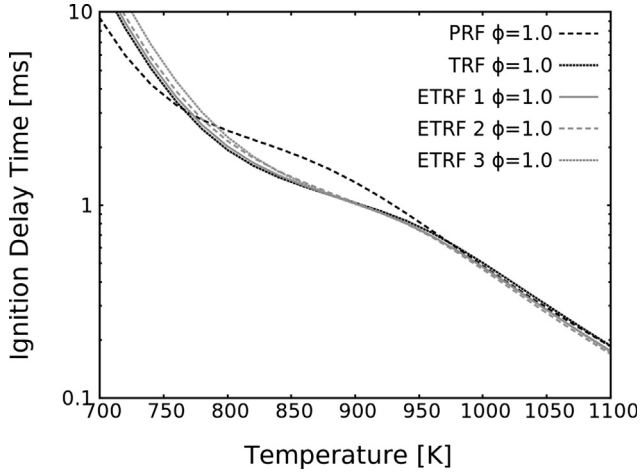

Fig. 6. Ignition delay time prediction of the surrogates for $\phi = 1$ at 60 bar using the skeletal scheme for auto-ignition prediction by Seidel [26].

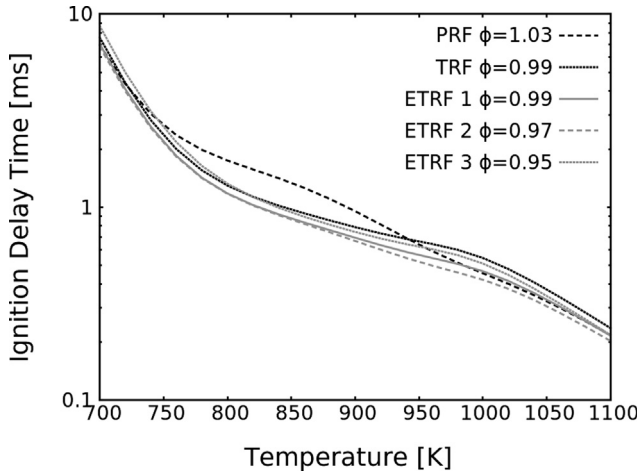

Fig. 7. Ignition delay time prediction of the surrogates for the actual ϕ in CFD at 60 bar using the skeletal scheme for auto-ignition prediction by Seidel [26].

milliseconds to crank angle degree assuming 2000 rpm (Fig. 8). At temperatures > 900 K, the differences in ignition delay are about 1 °CA and higher. This would suggest a distinctive deviation in KLSA in the engine simulations due to the surrogate formulation when only

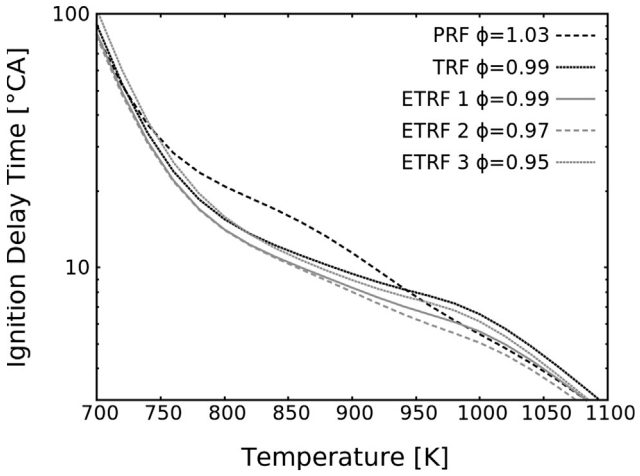

Fig. 8. Ignition delay time prediction in crank angle degree at 60 bar assuming a speed of 2000 rpm using the skeletal scheme for auto-ignition prediction by Seidel [26].

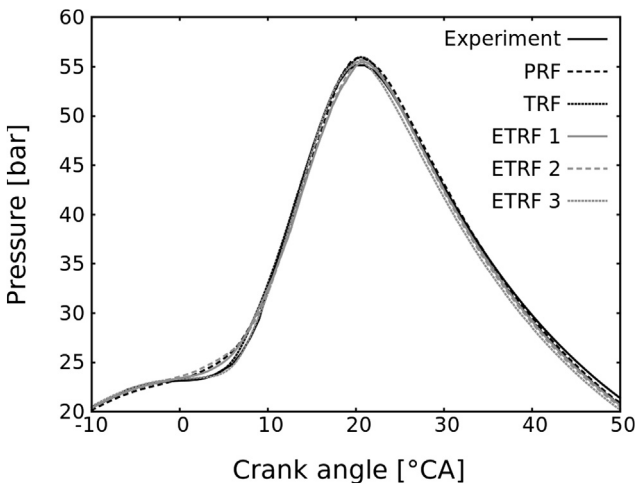

Fig. 9. Predicted mean pressure at the reference spark timing for the different surrogates using the same fuel mass and flame speed table.

considering ignition delay times.

The predicted mean pressure from CFD for the different surrogates at the reference (ref) spark timing from the experiment are shown in Fig. 9. Since the same flame speed table is used for all calculations the flame propagation prediction is similar and the thermodynamic conditions in the unburned zone are comparable. For all surrogates a spark sweep from −2 °CA to +1 °CA related to the reference spark timing is performed. Exemplary, the predicted maximum pressure in the cylinder is shown for the spark sweep using “ETRF 2” (Fig. 10). At TDC, the initialized spark is visible. Shortly before the maximum pressure is reached, fluctuations resulting from auto-ignitions in the unburned zone occur. The onset of those fluctuations delays and the amplitude decreases with delayed spark timing as it is expected from literature. For all calculated spark timings, the predicted auto-ignitions in the unburned zone are evaluated using the detonation diagram (Fig. 11). “ETRF 2” shows the strongest auto-ignition events in the developing detonation regime. For surrogate “TRF” and “PRF” the ignition kernels for ST −2 °CA are very close to the transition line and therefore accounted to the developing detonation regime. For surrogate “PRF” the auto-ignition onset is the latest. This agrees well with the theory since it has the highest MON. Surrogates “TRF” and “ETRF 1” differ in their composition, but have the same MON and fuel/air equivalence ratio in the engine simulation. However, the evaluation using the detonation

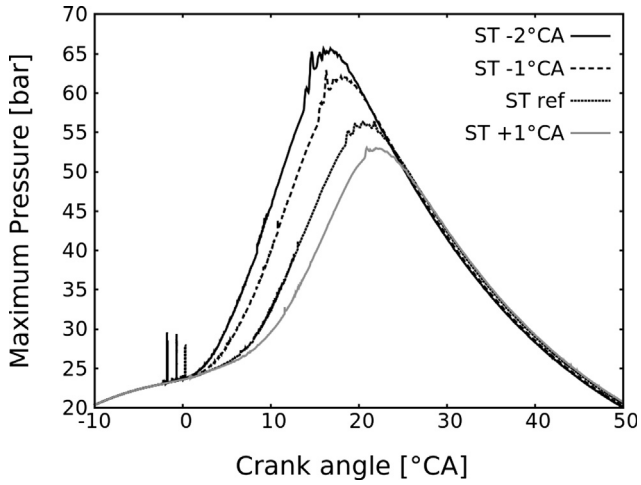

Fig. 10. Maximum predicted pressure for the spark timing sweep of "ETRF 2".

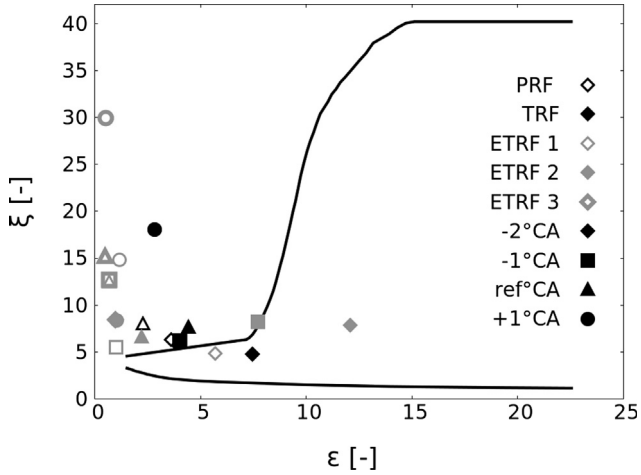

Fig. 11. Evaluation of the auto-ignitions predicted corresponding to Fig. 9 (same fuel mass and flame speed table) and the spark sweep in the detonation diagram.

diagram shows noticeable differences in the strengths of the auto-ignitions. Comparing the three ETRF surrogates, "ETRF 2" forms the strongest auto-ignition kernels and "ETRF 3" the weakest. This finding agrees with the trend in ignition delay time, but disagrees in terms of MON. "ETRF 3" has the lowest, "ETRF 1" the highest MON. Considering only this characteristic number the trends in auto-ignition tendency are unexpected. Several reasons might contribute to this finding: The suggested MON values for toluene differ in literature from MON = 104.0 [42] to MON = 109.0 [43]. To calculate the MON in this work MON = 109.0 is applied as it is reported by Heywood [1] and following the rules from Morgan et al. [13]. Further the difference in MON = 88.1 ("ETRF 1") and MON = 87.6 ("ETRF 2") are within the reproducibility and repeatability limits discussed in [3,42,43]. Additionally, the engine operating point with a boost pressure of 1.8 bar and 2000 rpm differs to the MON test conditions as discussed in [5–8]. The predicted ignition delay times > 820 K show a different trend in auto-ignition tendency than the MON numbers suggest (Figs. 7 and 8). "ETRF 2" leads to the biggest ignition kernels and highest maximum temperatures in those ignition kernels even though they are very similar in RON and MON. Moreover, effects from differences in fuel/air equivalence ratios, in heat capacity and local flow field may superpose the effect of MON. This becomes clearer when studying the kernel development of the "ETRF 3" surrogate.

Fig. 12 shows the dimensions of the ignition kernel using the low-temperature marker formaldehyde CH_2O, the propagation of the imposed reaction front using the hydroxyl radical OH as high-temperature marker and the imposed gas velocity as vector arrows. The level of CH_2O in the unburned zone in the time step prior to auto-ignition is the lowest for the PRF and increases with increasing *n*-heptane content, which has a pronounced low temperature chemistry, up to "ETRF 3". In those figures, it can also be seen that the ignition kernels appear in the same region for all calculations at reference spark timing thanks to the similar flame propagation and flow field prediction. The reactivity of the ignition kernels is illustrated using the mass fraction of OH and the gas velocity vectors. "ETRF 2" has clearly the strongest auto- ignition event. Surrogate "PRF" has an ignition kernel size that is similar to the ones of "TRF", "ETRF 1" and "ETRF 2", but is less reactive. Even though "ETRF 3" shows the highest concentration of the low temperature marker CH_2O, it shows the lowest concentration of *OH* and the smallest reacted burned volume (Fig. 12, bottom row center). There is less energy available in the ignition kernel due to the lower fuel/air equivalence ratio and lower LHV. At this crank angle, the energy released by auto-ignition competes against the quenching by expansion and it may be possible that the kernel cannot release sufficient energy needed to develop knocking combustion. Using surrogate "ETRF 2" and spark timing ST-2°CA a much stronger knock event than for the other surrogates and spark timings is predicted. This is because the position of the auto-ignition kernel changes. After the first ignition kernel on the side of the intake valves, the flame and the induced pressure gradient lead to a second stronger knock event close to the exhaust valves (Fig. 13).

4.3. Impact on engine knock prediction assuming constant fuel/Air equivalence ratio

In the next step, the different surrogates are initialized, and the flame speed table generated for the specific surrogates are applied. The fuel mass was adjusted to give the same fuel/air equivalence ratio ($\phi = 1 \pm 0.01$) for all surrogates. The results of this simulations are shown in Fig. 14. As observed in the flame speed analysis above (Fig. 4), surrogate "PRF" leads to the fastest flame propagation, "ETRF 3" to the slowest. To match the predicted peak pressure with the experiment, the spark timing was calibrated for the surrogates "PRF" and "ETRF 3". The necessary shift in spark timing is given in Table 5. The comparison of predicted pressure traces with reference and calibrated spark timing are shown in Figs. 14 and 15. The prediction of the peak pressure location and value is improved with adjusted spark timing (Tables 6 and 7). For the cases with adjusted spark timing the same analysis as for the cases with the same fuel mass has been performed.

Fig. 16 shows the evaluation in the detonation diagram of this study. Conspicuous is that "ETRF 2" leads to much weaker auto-ignitions than observed in Fig. 11. The ignition kernels occur in the same region (at the side of the intake valves). The transition of the strongest auto-ignition event to the exhaust valve side is not predicted. The ignition delay times in the charge with $\phi \pm 0.01$ are longer than in the previous studies $\phi = 0.97$ (Fig. 7). For surrogate "PRF" the same trend as in the previous study is found. The predicted auto-ignitions are the weakest in comparison to the other surrogates, the strongest auto-ignition (predicted for the spark timing ST -2 °CA) is clearly in deflagration mode. "TRF" and "ETRF 1" with the same MON, show a very different transition to a possible developing detonation. For surrogate "ETRF 1" the same transition of the strongest knock event as illustrated in Fig. 13 is predicted. Whereas for surrogate "TRF" with advanced spark timing ξ decreases and ε increases, for surrogate "ETRF 1", ξ decreases less. The same trends and reason for this can be found in the maximum temperatures in the ignition kernel just prior the high temperature ignition (Fig. 17).

Table 8 presents the auto-ignition onset and the latest spark timing of predicted knock for the two CFD studies. Whereas, except for the PRF, the auto-ignition onset is close for the complex surrogates, varies the tendency to form a developing detonation. The results show, that

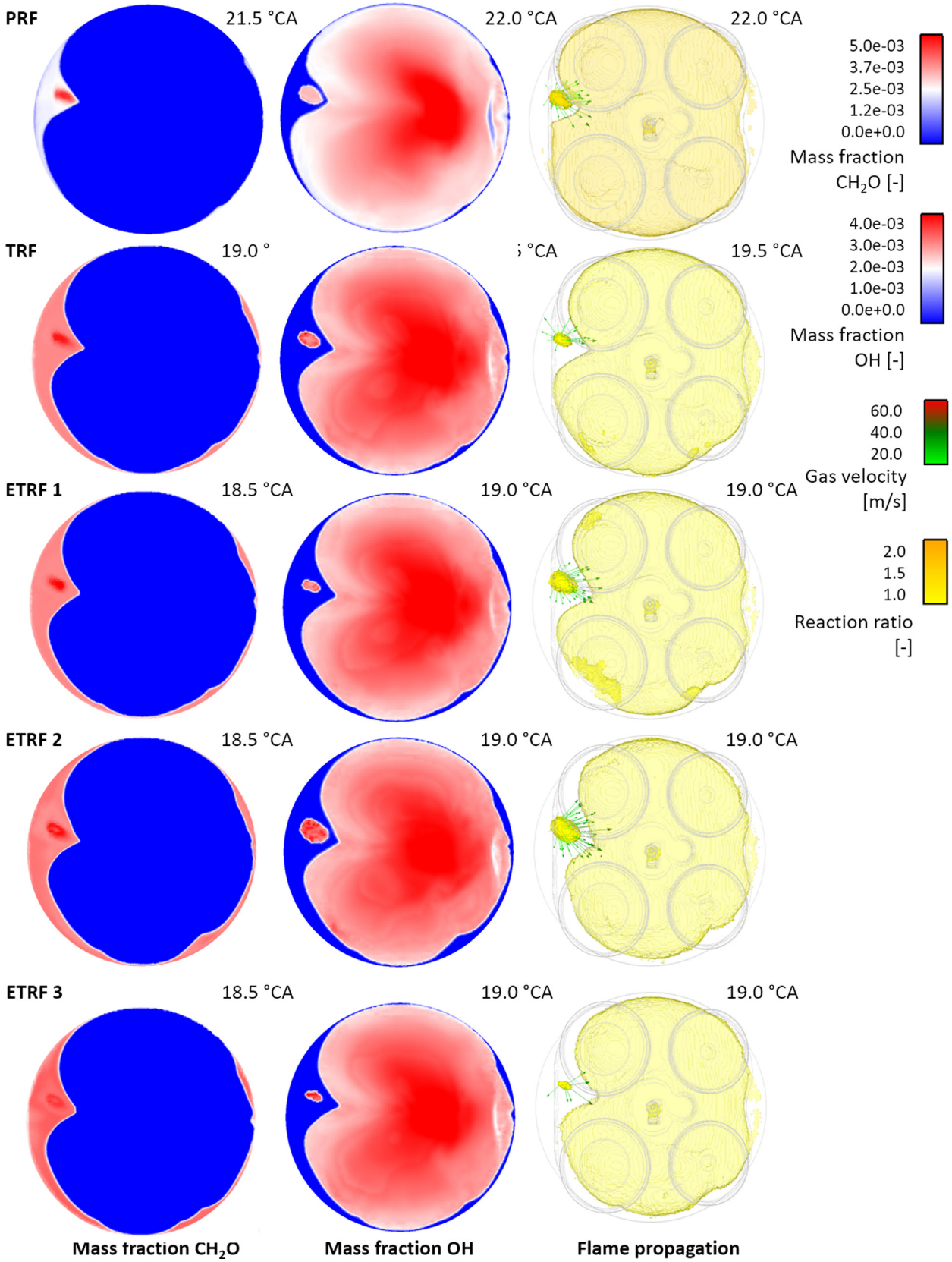

Fig. 12. Predicted ignition kernels for the different surrogates and the reference spark timing (corresponding to Fig. 9). View from top on a clip plane.

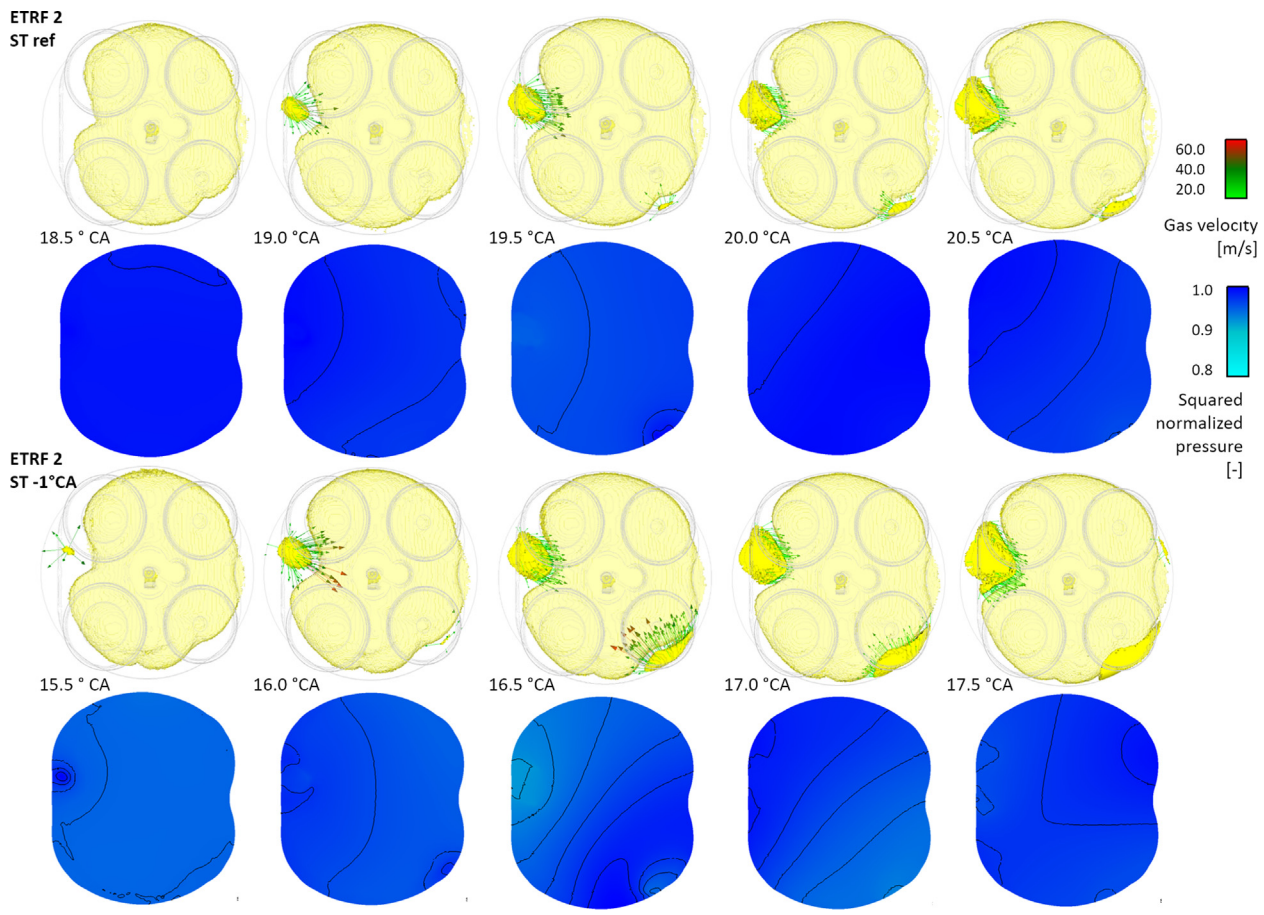

Fig. 13. Illustration of the transition of the strongest auto-ignition kernel from intake to exhaust valve side. Strength of the auto-ignition is presented by the imposed gas-velocity and the induced pressure gradients.

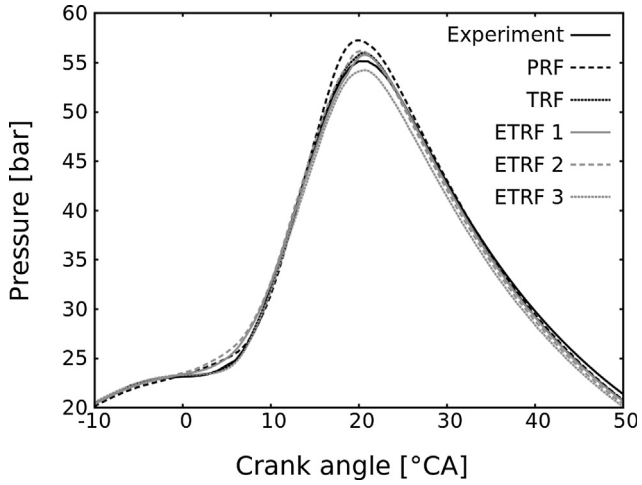

Fig. 14. Predicted mean pressure using the surrogate specific flame speed table and $\phi \pm 0.01$ at the reference spark timing.

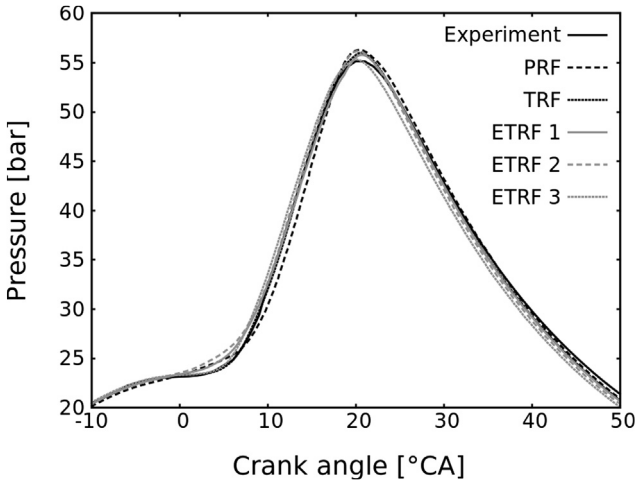

Fig. 15. Predicted mean pressure using the surrogate specific flame speed table and $\phi \approx 1$ at the calibrated spark timing (Table 5).

Table 5
Shift in spark timing to match the combustion process of the experiment.

PRF	TRF	ETRF 1	ETRF 2	ETRF 3
+2.0 °CA	–	–	–	−0.5°CA

even though a similar flame propagation and flow filed are predicted, the surrogates auto-ignite different. The ignition onset, kernel sizes as well as the imposed gas velocities differ between the surrogates. This finding is independent from the fuel/air equivalence ratio. The differences in KLSA due to the differences in the surrogate composition are found to be up to 2 °CA. The cooling due to vaporization may increase predicted differences. The ranking of the ETRF surrogates may depend on the properties used for the surrogate composition and the accuracies of the chemical and numerical models. However, it is evident that the

Table 6
Predicted location of the peak pressure and the combustion phasing related to the experiment. Analysis of the combustion prediction shown in Fig. 14.

		Experiment	PRF	TRF	ETRF1	ETRF2	ETRF3
CA_5	[°CA aTDC]	6.5	−0.3	0.2	−0.4	−0.9	0.3
CA_{10}	[°CA aTDC]	8.7	−0.2	−0.2	−0.6	−0.7	−0.2
CA_{50}	[°CA aTDC]	15.3	0.0	0.3	0.3	−0.1	0.2
CA_{90}	[°CA aTDC]	24.5	−1.5	0.6	−0.5	−1.4	−0.5
θ_{Pmax}	[°CA aTDC]	20.0	0.0	0.5	0.7	0.2	0.7
P_{max}	[MPa]	55.2	2.1	0.8	0.6	1.0	−1.0

Table 7
Predicted location of the peak pressure and the combustion phasing related to the experiment. Analysis of the combustion prediction shown in Fig. 15.

		Experiment	PRF	TRF	ETRF1	ETRF2	ETRF3
CA_5	[°CA aTDC]	6.5	−0.1	0.2	−0.4	−0.9	−0.2
CA_{10}	[°CA aTDC]	8.7	0.1	−0.2	−0.6	−0.7	−0.7
CA_{50}	[°CA aTDC]	15.3	0.5	0.3	0.3	−0.1	−0.3
CA_{90}	[°CA aTDC]	24.5	−0.9	0.6	−0.5	−1.4	−1.0
θ_{Pmax}	[°CA aTDC]	20.0	0.3	0.5	0.7	0.2	0.1
P_{max}	[MPa]	55.2	1.1	0.8	0.6	1.0	0.1

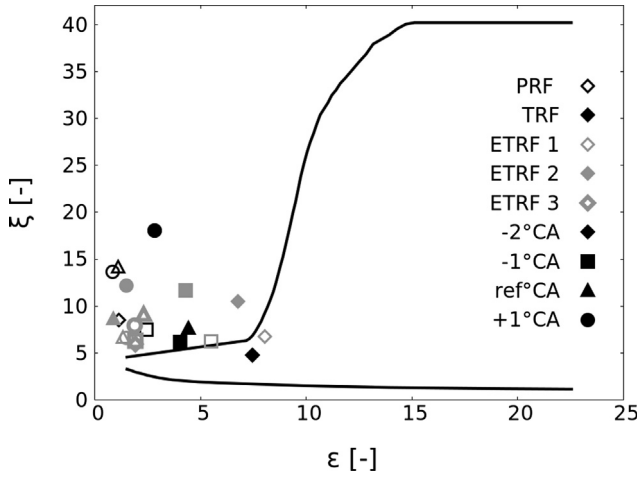

Fig. 16. Evaluation of the predicted auto-ignitions performing a spark variation corresponding to Fig. 15.

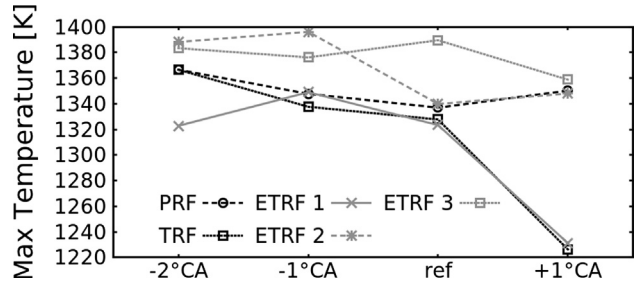

Fig. 17. Maximum predicted temperatures in the ignition kernel in the time step prior high temperature ignition.

predictions using the PRF surrogate are outliers. The auto-ignition onset is predicted later, the ignition event weaker. Using this simplified surrogate underestimates the knock tendency compared to the more complex surrogate formulations. This finding goes well together with the MON numbers. The discrepancy between the found results and the OI rating can be explained by omitting the injection and other operating factors such as the flow through the valves. However, in homogenous zero-dimensional reactors that are used for the development of reaction

Table 8
Predicted auto-ignition onset of the reference spark timing and latest spark timing of predicted knock corresponding to Figs. 11 and 16.

	First auto-ignition event [°CA]		First knock event [ST in °CA]	
	m_{fuel} = const	ϕ = const	m_{fuel} = const	ϕ = const
PRF	22.0	22.5	−2	\
TRF	19.5	20.0	−1	−1
ETRF 1	19.0	19.0	−2	−1
ETRF 2	19.0	18.5	−1	\
ETRF 3	19.0	19.5	\	\

mechanism and to validate against ignition delay time measurements those effects are also neglected. The conditions are closer to the MON test than to the RON test. To understand if the different knock tendency can be estimated with homogeneous reactors, so that computationally expensive CFD simulations can be avoided, the auto-ignition tendency of the surrogates is investigated in constant volume reactors (CVR) and zero-dimensional rapid compression machine (RCM) simulations.

4.4. Comparison to homogenous zero-dimensional simulations

Fig. 18 shows the mass fractions of the low-temperature species CH_2O, an early *iso*-octane decomposition product $C_8H_{17,}$ the temperature marker OH and the temperature of the domain. The species mass and temperature profiles are shown for different simulation methods:

a) Constant volume reactors (CVR) that are typically used to calculate ignition delay times at 800 K and 60 bar. Simulations have been performed for all surrogates with ϕ = 1.0.
b) As a) but using the mixtures when keeping the surrogate mass constant and ϕ varies between 1 ± 0.05.
c) Homogeneous rapid compression machine (RCM) simulations imposing the engine volume profile and initial species concentrations as in the engine simulation to consider the transient effects. Calculations with an initial temperature of 600 K do not ignite, but show the evolution of the low temperature chemistry.
d) As c), but with an initial temperature of 800 K to study auto-ignition.
e) 3D CFD SI engine simulations with constant fuel mass.

The ignition delay time estimated from the OH gradient ranks the auto-ignition tendency. If no auto-ignition is predicted, the surrogate with the highest concentration of low temperature species, earliest formation of OH and the highest compression end temperature is assumed to auto-ignite the first, the others in descending order. For the CFD simulation, the ranking from auto-ignition onset (AI onset) and the evaluation from the detonation diagram are shown.

The auto-ignition tendency of the surrogates differs in the predicted order as well as in sensitivity. In the CVR simulations the maximum deviation, expressed in crank angle degree assuming 2000 rpm, is 2.0 °CA, in the RCM simulations it is 1.0 °CA. Analyzing the same operating point with the ETRF mechanism by Cai and Pitsch [44] leads to maximum deviations of 4.0 °CA and 1.5 °CA, respectively. This deviation is proportional with speed. The stationary CVR simulations are more sensitive to changes in the chemistry than the RCM simulations, in which pressure and unburned temperatures change. The CVR simulations are therefore more meaningful to understand the differences in ignition delay. In contrast, the RCM simulations give the conclusion that differences between CVR and CFD rankings are not only explained by transient effects. In both simulations where auto-ignition is observed (CVR a) and RCM d)), the low temperature chemistry occurs the earliest for surrogate "PRF", which is not the case in the transient and non-igniting RCM and in the mean CFD simulation output (Fig. 18, bottom row). The CH_2O concentration is lower as for the other surrogates as it

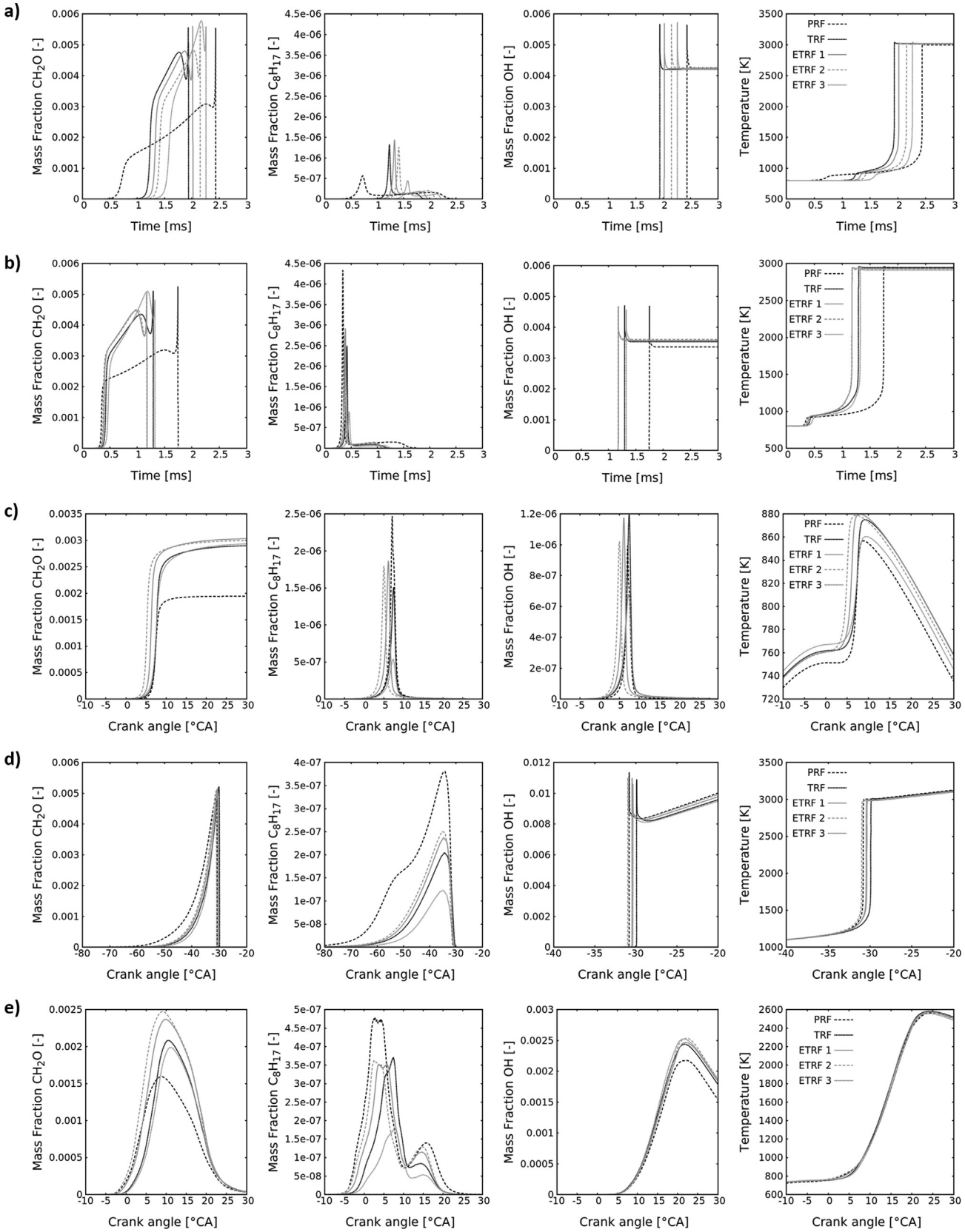

Fig. 18. Predicted mass fractions of typical low temperature species (CH_2O, C_8H_{17}) and high chemistry species (OH) and temperature profiles for different simulation methods. a) CVR simulation with 800 K, 60 bar and $\phi = 1$. b) CVR simulation with 800 K, 60 bar, $\phi_{PRF} = 1.03$, $\phi_{TRF} = 0.99$, $\phi_{ETRF1} = 0.99$, $\phi_{ETRF1} = 0.97$ and $\phi_{ETRF1} = 0.95$. c) RCM simulation with a initial temperature of 600 K, ϕ as in b). d) RCM simulation with an initial temperature of 800 K, ϕ as in b).e) CFD simulation average ϕ as in b).

Table 9
Auto-ignition tendency estimated from MON rating (for these surrogates equivalent to AKI ranking), OI assuming K = −0.5 and different simulation methods and RCM[1] is initialized with 600 K, RCM[2] with 800 K and Knock tendency from CFD.

	ϕ	Auto-ignition tendency ranking								
MON		ETRF 3	>	ETRF 2	>	ETRF 1	|	TRF	>	PRF
OI		PRF	>	TRF	|	ERTF 1	>	ETRF 2	>	ETRF 3
CVR	1.0	TRF	>	ETRF 1	>	ETRF 2	>	ETRF 3	>	PRF
CVR	1 ± 0.05	ETRF 1	|	ETRF 2	>	TRF	>	ETRF 3	>	PRF
RCM[1]	1 ± 0.05	ETRF 2	>	ETRF 1	>	TRF	|	ETRF 3	>	PRF
RCM[2]	1 ± 0.05	ETRF 2	>	PRF	>	ETRF 1	|	ETRF 3	>	TRF
CFD (AI onset)	1 ± 0.05	ETRF 1	|	ETRF 2	|	ETRF 3	>	TRF	>	PRF
CFD (AI onset)	1 ± 0.01	ETRF 2	>	ETRF 1	>	ETRF 3	>	TRF	>	PRF
		Knock tendency ranking								
CFD (knock)	1 ± 0.05	ETRF 2	>	TRF	>	ETRF 1	>	PRF	>	ETRF 3
CFD (knock)	1 ± 0.01	TRF	>	ETRF 1	>	ETRF 2	>	PRF	|	ETRF 3

is also predicted in the transient simulations. “ETRF 2” has the earliest CH_2O formation in the transient calculations and leads to the strongest knock events in the CFD simulation. “ETRF 1” has a lower tendency to auto-ignite than “ETRF 2” in the RCM and CFD simulation, but not in the CVR calculations. From the RCM calculation, it can be seen that “ETRF 3” reaches a higher compression pressure and temperature, but releases the least energy in the expansion. The TRF mixture has longer ignition delay times in the CVR calculations, but is on the second rank in knock tendency in the engine simulation. This points out, that solely from homogeneous calculations (CVR or RCM) no conclusion on the knock tendency can be drawn from this setup.

The same study was performed using the ETRF mechanism from Cai and Pitsch [44]. Even though this scheme ignites earlier, the same trends for the ETRF surrogates have been found, and no clear connection between the homogeneous calculations and the knock tendency in the CFD calculation was found. In literature, studies relating ignition delay times from 0D simulations to the octane rating can be found. They emphasize that their relation is not straight forward, e.g. [45]. The different auto-ignition tendencies are ranked in Table 9. It needs to be pointed out, that this ranking depends on the initial temperature and pressure. As it can be seen from Figs. 6 to 8, the predicted ignition delay time of surrogate “PRF” crosses the predicted ignition delay times of the other surrogates in the range from 900 K to 1050 K. However, as demonstrated this also changes with the applied model approach (transient in the RCM or stationary in the CVR simulations). Small changes in fuel/air equivalence ratio (Fig. 18a) and b)) lead to a different ranking. In the CFD simulations, local gradients in unburnt temperature as well as species concentrations are predicted. Those gradients affect the occurrence of predicted of the auto-ignition events.

Overall surrogate “ETRF 2” is ranked to auto-ignite the most likely, “PRF” is ranked to be the most auto-ignition resistant. Not every auto-ignition leads to engine knock. It is essential to distinguish a harmless auto-ignition in deflagration mode from an auto-ignition that leads to a developing detonation. The comparison of the AI onset and knock tendency of the different CFD simulations show this. Regarding the AI onset only, the TRF and ETRF surrogates are close; the ranking in terms of the transition to developing combustion shows bigger deviations. “ETRF 3” ignites in the same crank angle, but does not from a developing detonation. By considering the ignition delay times from homogenous stationary or transient simulations, this distinction cannot be made since no gradients in temperature or ignition delay time are present. For this kind of analysis, simulation approaches that account for inhomogeneity are necessary, i.e. CFD simulations or zero-dimensional stochastic reactor models [32,46,47]. Fig. 12 shows that even though the auto-ignition is predicated in the same time step (ETRF surrogates), only “ETRF 2” turns to a developing detonation. This conclusion cannot be drawn from a homogenous calculation.

5. Conclusions

Surrogates with same RON, but different number of surrogate species and compositions have been composed. The surrogates therefore differ in MON, LHV, C:H:O-ratio, density and other properties. The surrogates have been compared regarding their flame propagation and auto-ignition prediction. The auto-ignition prediction was analyzed first for the same fuel mass and second for the same fuel/air equivalence ratio. Further, the auto-ignition tendency was investigated using constant volume reactor and rapid compression machine simulations.

Summarizing this study, it was found that even though the surrogates have the same RON, the tendency to auto-ignite in the engine simulations is very different. No clear connections between MON and knock tendency or ignition delay time in homogeneous reactors and knock tendency was found. The predicted sensitivities may also depend on the specific surrogate properties and the resulting small differences in the initial charge such as density, heat capacity, LHV and C:H:O-ratio. It was found that it is not possible to estimate the knock tendency of different surrogates in the CFD simulation from homogeneous reactor calculations. The ranking in terms of auto-ignition onset and transition to developing detonation are different, since not every auto-ignition turns to engine knock. This finding is irrespective of the used reaction scheme, but may be influenced by the physical properties of the analyzed surrogates. There is a complex interaction between turbulence, physical phenomena and combustion chemistry.

Acknowledgement

Convergent Science, Inc is thanked for providing the licenses used for this analysis.

Appendix

Surrogate formulation

Seidel [26] developed a surrogate formulation method based on published correlations from Morgan et al. [13] and Anderson et al. [41]. The correlation from Morgan et al. [13] is used to formulate the toluene reference fuel (TRF) surrogate for the gasoline fraction. The linear by molar fraction mixing rule for oxygenated fuels with gasoline suggested by Anderson et al. [41] is applied to determine the impact of the ethanol fraction. To compose the surrogates, the aromatic content is represented by toluene. The ethanol fraction and the RON of the gasoline are imposed as well.

Table A1
Coefficients for the calculation of octane rating and the composition of a surrogate [13].

Coefficient	$a_{x,P}$	$a_{x,tol}$	$a_{x,tol2}$	$a_{x,tol,P}$
RON (x = R)	100.0	142.79	−22.651	−111.95
MON (x = M)	100.0	128.00	−19.207	−119.24
S (x = S)	0.0	14.79	−3.444	7.29

Table A2
Properties of the surrogate species [26].

Species	Formula	RON [–]	MON [–]	Density [kg/m^3]	LHV [MJ/kg]
iso-octane	C_8H_{18}	100.0	100.0	692.0	44.4
n-heptane	C_7H_{16}	0.0	0.0	683.8	44.6
toluene	C_7H_8	120.0	109.0	866.9	40.6
ethanol	C_2H_5OH	109.0	90.0	789.7	28.9

Table A3
Measured properties of various commercial gasolines [26].

	RON [–]	MON [–]	Aromates [vol.%]	Ethanol [vol.%]	ρ [kg/m3]	C [w%]	H [w%]	O [w%]	LHV [MJ/kg]
1	93.6	82.4	11.7	22.8	744.0	77.7	13.9	8.4	39.6
2	96.7	85.8	27.9	9.5	744.0	83.0	13.5	3.5	41.5
3	95.6	84.0	22.8	0.0	746.0	84.1	13.6	2.3	42.4
4	96.2	85.1	36.9	0.0	763.7	84.8	12.8	2.4	42.9
5	91.0	81.2	26.2	0.0	747.4	84.3	13.4	2.3	44.4
6	91.4	82.4	37.0	0.0	761.5	84.9	12.9	2.2	44.4
7	87.9	80.5	36.3	0.0	751.7	86.8	13.2	< 0.2	NA
8	> 95.0	> 85.0	0.0	95.8	808.0	48.8	12.9	38.3	25.0
9	87.0	77.5	24.0	0.0	744.2	86.8	13.4	< 0.2	43.2
10	90.1	80.2	26.3	0.0	753.0	86.7	13.3	0.0	43.1
11	94.0	80.9	26.2	0.0	750.6	84.4	13.2	2.4	42.0
12	106.9	95.3	35.2	0.0	756.2	84.1	12.7	3.2	41.3
13	91.0	82.0	14.9	0.0	744.2	86.0	14.0	< 0.1	43.5
14	94.5	84.1	32.6	0.0	747.5	86.9	13.1	< 0.2	42.9

Table A4
Properties of the surrogates corresponding to the commercial gasolines in Table A2 [26].

	RON [–]	MON [–]	ethanol [w%]	toluene [w%]	iso-octane [w%]	n-heptane [w%]	ρ [kg/m3]	C [w%]	H [w%]	O [w%]	LHV [MJ/kg]
1	93.6	83.5	25.0	13.1	45.7	16.2	746.0	77.0	14.4	8.7	39.5
2	97.7	88.1	10.1	32.0	46.0	11.9	752.0	83.1	13.4	3.5	41.3
3	95.6	91.0	0.0	27.1	63.1	9.9	730.6	86.0	14.0	0.0	43.3
4	96.2	89.1	0.0	42.4	45.9	11.7	754.9	87.1	12.9	0.0	42.8
5	91.0	85.9	0.0	30.9	54.2	15.0	735.8	86.2	13.8	0.0	43.2
6	91.4	84.5	0.0	42.5	41.1	16.4	754.4	87.1	13.0	0.0	42.8
7	87.9	81.2	0.0	41.8	38.5	19.7	752.8	87.0	13.0	0.0	42.8
8	108.0	89.3	96.6	0.0	1.5	1.9	787.7	53.3	13.2	33.6	27.4
9	87.0	82.4	0.0	28.4	53.1	18.4	731.5	86.0	14.0	0.0	43.3
10	90.1	85.0	0.0	31.0	53.2	15.9	735.9	86.2	13.8	0.0	43.2
11	94.0	88.8	0.0	30.6	57.3	12.0	753.8	86.3	13.7	0.0	43.2
12	106.9	99.6	0.0	40.5	57.5	2.0	753.3	87.1	12.9	0.0	42.8
13	91.0	88.0	0.0	18.0	69.3	12.7	716.4	85.4	14.6	0.0	43.7
14	94.5	88.2	0.0	37.8	49.5	12.7	747.3	86.8	13.2	0.0	42.9

The *iso*-octane and *n*-heptane fractions of the surrogate are calculated to match the RON of the gasoline. To correlate the TRF mixture a re-normalization of the PRF mixture from the space [0,100] to [0,1] is needed. Since the RON of a PRF is directly given by the mole fraction of *iso*-octane X_{oct} and *n*-heptane X_{hept}, the renormalization is given by [13]:

$$P = \frac{X_{iso}}{X_{iso} + X_{hept}} \tag{A1}$$

The Modified Linear by Volume (MLbV) approximation for the RON of a TRF mixture is [13]:

$$RON = a_{R,P}P + a_{R,tol}X_{tol} + a_{R,tol2}X_{tol}^2 + a_{R,tol,P}X_{tol}P \tag{A2}$$

To find the composition of a TRF surrogate with a specific toluene content, RON and the surrogate sensitivity, the MLbV method can be inverted. The following equations result [13] (the coefficients are listed in Table A1):

$$P = \frac{RON - a_{R,tol}X_{tol} + a_{R,tol2}X_{tol}^2}{100 + a_{R,tol,P}X_{tol}} \tag{A3}$$

$$S = a_{S,tol}X_{tol} + a_{S,tol2}X_{tol}^2 + \frac{a_{S,tol,P}X_{tol}(RON - a_{R,tol}X_{tol} + a_{R,tol2}X_{tol}^2)}{100 + a_{R,tol,P}X_{tol}} \tag{A4}$$

To respect the ethanol content, the linear molar based blending rule, in detail investigated and extended by a scaling parameter P_g by Anderson et al. [41], is applied. In this approach, the octane rating ON (valid for both RON and MON) are mixed based on the ethanol mole fraction X_{eth} [41]:

$$ON_{blend} = (1 - X_{eth})ON_{gas} + (1 - X_{eth})ON_{eth} + P_g X_{eth}(1 - X_{eth})(ON_{eth} - ON_{gas}) \tag{A5}$$

P_g is a scaling parameter that needs to be determined from measurement. In case *Pg* is not known, it is set to $P_g = 0$, so that the last term in Eq. (A5) is neglected. The surrogates are composed using the properties in Table A2. Once the ETRF surrogate is defined, physical and chemical properties of the surrogate such as C:H:O-ratio, MON, lower heating value (LHV) and density can be calculated in close agreement with the commercial gasoline fuels. The validation and agreement to commercial gasoline can be found in detail in [26] and in Tables A3 and A4.

References

[1] Heywood JB. Internal combustion engine fundamentals. McGraw-Hill Education; 1988.
[2] Ricardo HR. Schnellaufende Verbrennungsmaschinen. Heidelberg: Springer-Verlag GmbH; 1926.
[3] Merker GP, Schwarz C, Teichmann R. Combustion engines development: mixture formation, combustion, emissions and simulation. Springer-Verlag Berlin Heidelberg; 2012.
[4] Leppard WR. The chemical origin of fuel octane sensitivity. SAE Tech Pap 1990. 902137.
[5] Prakash A, Wang C, Janssen A, Aradi A, Cracknell R. Impact of Fuel Sensitivity (RON-MON) on Engine Efficiency. SAE Int J Fuels Lubr 2017;10:115–25.
[6] Kalghatgi GT. Fuel anti-knock quality – Part I. Engine studies. SAE Tech Pap 2001. 2001-01-3584.
[7] Kalghatgi GT. Fuel anti-knock quality – Part II. Vehicle studies – how relevant is motor octane number (MON) in modern engines? SAE Tech Pap 2001.
[8] Yates ADB, Swarts A, Viljoen CL. Correlating auto-ignition delays and knock-limited spark-advance data for different types of fuel. SAE Tech Pap 2005. 2005-01-2083.
[9] Halstead MP, Kirsch LJ, Quinn CP. The autoignition of hydrocarbon fuels at high temperatures and pressures – fitting of a mathematical model. Combust Flame 1977;30:45–60.
[10] Sazhin SS, Sazhina EM, Heikal MR, Marooney C, Mikhalovsky SV. The shell auto-ignition model: a new mathematical formulation. Combust Flame 1999;117(3):529–40.
[11] Sazhina EM, Sazhin SS, Heikal MR, Marooney CJ. The shell autoignition model: applications to gasoline and diesel fuels. Fuel 1999;78(4):389–401.
[12] Teodosio L, De Bellis V, Bozza F. Fuel economy improvement and knock tendency reduction of a downsized turbocharged engine at full load operations through a low pressure EGR system. SAE Int J Engines 2015;8:1508–19.
[13] Morgan N, Smallbone A, Bhave A, Kraft M, Cracknell R, Kalghatgi GT. Mapping surrogate gasoline compositions into RON/MON space. Combust Flame 2010;157(6):1122–31.
[14] Gauthier BM, Davidson DF, Hanson RK. Shock tube determination of ignition delay times in full-blend and surrogate fuel mixtures. Combust Flame 2004;139(4):300–11.
[15] Andrae JCG, Björnbom P, Cracknell RF, Kalghatgi GT. Autoignition of toluene reference fuels at high pressures modeled with detailed chemical kinetics. Combust Flame 2007;149(1):2–24.
[16] Stenlåås O, Gogan A, Egnell R, Sundén B, Mauss F. The influence of nitric oxide on the occurrence of autoignition in the end gas of spark ignition engines. SAE Tech Pap 2002. 2002-01-2699.
[17] Hoffmeyer H, Montefrancesco E, Beck L, Willand J, Ziebart F, Mauss F. CARE – CAtalytic Reformated Exhaust Gases in turbocharged DISI-engines. SAE Int J Fuels Lubr 2009;2:139–48.
[18] Gülder OL. Correlations of laminar combustion data for alternative S.I. engine fuels. SAE Tech Pap 1984.
[19] Metghalchi M, Keck JC. Burning velocities of mixtures of air with methanol, iso-octane, and indolene at high pressure and temperature. Combust Flame 1982;48:191–210.
[20] Peters N. Turbulent combustion. Cambridge University Press; 2000.
[21] Richards KJ, Senecal PK, Pomraning E. CONVERGE v2.4 manual. Convergent Science, Inc.; 2017.
[22] Liang L, Reitz RD. Spark ignition engine combustion modeling using a level set method with detailed chemistry. SAE Tech Pap 2006. 2006-01-0243.
[23] Perini F, Ra Y, Hiraoka K, Nomura K, Yuuki A, Oda Y, et al. An efficient level-set flame propagation model for hybrid unstructured grids using the G-equation. SAE Int J Engines 2016;9:1409–24.
[24] Tan Z, Reitz RD. Modeling ignition and combustion in spark-ignition engines using a level set method. SAE Tech Pap 2003. 2003-01-0722.
[25] Pal P, Wu Y, Lu T, Som S, See Y, Le Moine A. Multi-dimensional CFD simulations of knocking combustion in a CFR engine. Emissions control systems; instrumentation, controls, and hybrids; numerical simulation; engine design and mechanical development: V002T06A017. Internal Combustion Engine Division Fall Technical Conference 2017;Volume 2.
[26] Seidel L. Development and reduction of a multicomponent reference fuel for gasoline PhD thesis Brandenburg University of Technology Cottbus-Senftenberg; 2017
[27] Seidel L, Moshammer K, Wang X, Zeuch T, Kohse-Höinghaus K, Mauss F. Comprehensive kinetic modeling and experimental study of a fuel-rich, premixed n-heptane flame. Combust Flame 2015;162(5):2045–58.
[28] Ahmed SS, Mauss F, Moréac G, Zeuch T. A comprehensive and compact n-heptane oxidation model derived using chemical lumping. Phys Chem Chem Phys 2007;9:1107–26.
[29] Zeuch T, Moréac G, Ahmed SS, Mauss F. A comprehensive skeletal mechanism for the oxidation of n-heptane generated by chemistry-guided reduction. Combust Flame 2008;155(4):651–74.
[30] Seidel L, Netzer C, Hilbig M, Mauss F, Klauer C, Pasternak M, et al. Systematic reduction of detailed chemical reaction mechanisms for engine applications. J Eng Gas Turb Power 2017;139:091701–91709.
[31] Netzer C, Seidel L, Pasternak M, Lehtiniemi H, Perlman C, Ravet F, et al. Three-dimensional computational fluid dynamics engine knock prediction and evaluation based on detailed chemistry and detonation theory. Int J Engine Res 2018;19(1):33–44.
[32] Netzer C, Seidel L, Pasternak M, Klauer C, Perlman C, Ravet F, et al. Engine knock prediction and evaluation based on detonation theory using a quasi-dimensional stochastic reactor model. SAE Tech Pap 2017. 2017-01-0538.
[33] Bradley D, Morley C, Gu XJ, Emerson DR. Amplified pressure waves during auto-ignition: relevance to CAI engines. SAE Tech Pap 2002. 2002-01-2868.
[34] Bradley D, Kalghatgi GT. Influence of auto-ignition delay time characteristics of different fuels on pressure waves and knock in reciprocating engines. Combust Flame 2009;156(12):2307–18.
[35] Kalghatgi GT, Bradley D. Pre-ignition and 'super-knock' in turbo-charged spark ignition engines. Int J Engine Res 2012;13(4):399–414.
[36] Gu XJ, Emerson DR, Bradley D. Modes of reaction front propagation from hot spots. Combust Flame 2003;133(1):63–74.
[37] Zhen X, Wang Y, Xu S, Zhu Y, Tao C, Xu T, et al. The engine knock analysis – an overview. Appl Energy 2012;92:628–36.
[38] Peters N. Mega-knock in super-charged gasoline engines interpreted as a localized developing detonation. 4th conference knocking in gasoline engines, Berlin, 9–10 October 2013. IAV Automotive Engineering GmbH; 2013. p. 23–40.
[39] Bates L, Bradley D, Paczko G, Peters N. Engine hot spots: modes of auto-ignition and reaction propagation. Combust Flame 2016;166:80–5.
[40] LOGEsoft v1.10, LOGE AB. Available from: http://www.logesoft.com, 2018.
[41] Anderson JE, Leone TG, Shelby MH, Wallington TJ, Bizub JJ, Foster M, et al. Octane numbers of ethanol-gasoline blends: measurements and novel estimation method from molar composition. SAE Tech Pap 2012. 2012-01-1274.
[42] Spausta F. Eigenschaften und Untersuchungen der flüssigen Treibstoffe: die gasförmigen Treibstoffe. second ed. Wien: Springer-Verlag; 1953.
[43] Knop V, Loos M, Pera C, Jeuland N. A linear-by-mole blending rule for octane numbers of n-heptane/iso-octane/toluene mixtures. Fuel 2014;115:666–73.
[44] Cai L, Pitsch H. Optimized chemical mechanism for combustion of gasoline surrogate fuels. Combust Flame 2011;162(5):1623–37.
[45] Naser N, Sarathy SM, Chung SK. Estimating fuel octane numbers from homogenous gas-phase ignition delay times. Combust Flame 2018;188:307–23.
[46] Gogan A, Sundén B, Lehtiniemi H, Mauss F. Stochastic model for the investigation of the effect of inhomogeneities on engine knock. Internal combustion engine division fall technical conference. ASME; 2004.
[47] Gogan A, Sundén B, Lehtiniemi H, Mauss F. Stochastic model for the investigation of the influence of turbulent mixing on engine knock. SAE Tech Pap 2004. 2004-01-2999.